

## Electrical contact considerations for diamond electron emission diodes

Franz A. Koeck<sup>1)\*</sup>, Manpuneet Benipal<sup>2)</sup>, Robert J. Nemanich<sup>1)</sup>

*1) Department of Physics, Arizona State University, Tempe, AZ 85287 USA*

*2) Advent Diamond Inc., Scottsdale AZ, 85287 USA*

*\*Franz.Koeck@asu.edu*

### Abstract:

The demonstration of diamond devices has substantiated the superior capability of diamond in high power electronics that relied on the preparation of p-type and n-type diamond through boron and phosphorus doping, respectively, and the growth of high purity intrinsic diamond. We present an approach for electrical contacts to homoepitaxial, phosphorus doped, n-type, diamond that utilizes an interfacial layer of highly nitrogen doped, nanostructured carbon grown by plasma enhanced CVD (PECVD). This contact strategy was utilized in a pin diamond diode for electron source applications. The pin-nano-carbon structure was prepared on HPHT type IIb (111) oriented substrates with intrinsic, n-type, and nano-carbon layer grown in dedicated PECVD systems. The nanostructured nitrogen doped carbon layer was synthesized under argon addition to promote re-nucleation. Diodes from this pin-nano-carbon structure were prepared by lithography and mesa-etched devices contacted by Ti/Pt/Au metallurgy. Final processing in a hydrogen plasma established negative electron affinity properties for electron emission. Electrical characterization of the diodes commenced in vacuum after annealing at ~600°C for 15min and observation of exciton light emission indicated bipolar transport. At a forward bias of 14V a current of 0.1A was measured and at 17V its increase to 0.5A corresponded to a current density >1500A/cm<sup>2</sup>. Compared to conventional pin diodes, the introduction of the nano-carbon layer enhanced the diode and electron emission current by more than an order of magnitude. This was attributed to the reduced contact resistivity of  $5.5 \times 10^{-3} \Omega \text{ cm}^2$  at room temperature. Light emission and diode operation at temperatures >750°C indicated superior stability of the electrical contact. The n-type layer was characterized by SIMS indicating a phosphorus incorporation of  $\sim 2 \times 10^{19} \text{ cm}^{-3}$  and the nano-carbon layer a nitrogen incorporation of  $\sim 5 \times 10^{20} \text{ cm}^{-3}$ . Addressing contact limitations to n-type diamond through the growth of moderately phosphorus **doped** epilayers followed by highly nitrogen doped nano-carbon layers could provide a preferred approach for electronic devices that could also be extended to (100) surfaces.

### 1. Introduction

Continued interest in diamond electronics is based on the superior materials properties that could enable high power devices not possible with conventional semiconductor and other wide band-gap materials. Table 1 details selected materials properties for typical wide band-gap semiconductor

materials, including  $\beta$ -Ga<sub>2</sub>O<sub>3</sub> as an emerging semiconductor and in a comparison with diamond. Power devices based on diamond would be improved through the wide band-gap and increased breakdown voltage, high carrier mobilities and increased thermal conductivity. Stability at high temperatures would furthermore allow operation of diamond devices in extreme ambients.

		Si	4H-SiC	$\beta$ -Ga <sub>2</sub> O <sub>3</sub>	GaN	Diamond
<b>Bandgap</b>	<b>E<sub>g</sub> (eV)</b>	1.1	3.26	4.5-4.9	3.39	<b>5.45</b>
<b>Electron Concentration</b>	<b>n<sub>i</sub> (cm<sup>-3</sup>)</b>	1.5x10 <sup>10</sup>	8.2x10 <sup>-9</sup>		1.9x10 <sup>-10</sup>	<b>1.6x10<sup>-27</sup></b>
<b>Electron Mobility (high)</b>	<b><math>\mu_n</math> (cm<sup>2</sup>/V s)</b>	1450	950	300	1200	<b>4500</b>
<b>Hole Mobility (high)</b>	<b><math>\mu_p</math> (cm<sup>2</sup>/V s)</b>	430	120		200	<b>3800</b>
<b>Electron Saturation Velocity</b>	<b>v<sub>sat</sub> (10<sup>7</sup> cm/s)</b>	1	2	1.3	2.5	<b>1.5</b>
<b>Hole Saturation Velocity</b>	<b>v<sub>sat</sub> (10<sup>7</sup> cm/s)</b>	0.4	1		1.7	<b>1.1</b>
<b>Breakdown Electric Field</b>	<b>E<sub>br</sub> (MV/cm)</b>	0.3	3	8	3.3	<b>10</b>
<b>Thermal Conductivity</b>	<b>k (W/cm K)</b>	1.5	4.9	0.11-0.27	2.3	<b>20</b>
<b>Maximum Operating Temperature</b>	<b>T<sub>max</sub> (°C)</b>	175	500		650	<b>700</b>
<b>Johnson's figure of merit</b>		1	410		280	<b>8200</b>
<b>Baliga's figure of merit</b>		1	290	3444	910	<b>17200</b>

Table 1. Selected materials properties for various wide band-gap semiconductors where Johnson's figure of merit corresponds to the power-frequency product and Baliga's figure of merit to the conduction losses in lower frequency unipolar devices. [1]

Practical devices require suitable electrical contacts as they can present a limiting factor to solid state electronics and contribute to the on-resistance,  $R_{on}$ , an important parameter for devices. For power devices, a specific contact resistance  $<1 \times 10^{-5} \Omega \text{ cm}^2$  is typically required and higher frequency operation in the tera-hertz regime necessitates a further reduction to  $1 \times 10^{-8} \Omega \text{ cm}^2$ . [2, 3] As a load current  $I_{Load}$  passes through the device, power is dissipated ( $P_D$ ) as heat energy in the amount of  $P_D = I_{Load}^2 \times R_{on}$ . Minimizing these losses will result in operation at lower temperatures thus increasing efficiency and enabling more compact systems design. In a detailed report, elsewhere, the specific on-resistance  $R_{sp}$  for silicon and silicon carbide with respect to the breakdown voltage,  $V_B$ , was derived to  $R_{sp,Si} = 4.99 \times 10^{-4} \cdot V_B [\text{m} \Omega \cdot \text{cm}^2]$  and  $R_{sp,SiC} = 3.79 \times 10^{-6} \cdot V_B [\text{m} \Omega \cdot \text{cm}^2]$ , respectively. [4] Based on these relations, SiC can improve the specific on-resistance over Si by about 2 orders of magnitude. With an increase in the operating temperature an increase in the on-resistance is observed for SiC (for a 1000V diode operating at 250° C,  $R_{on}$  is increased by a factor of 5) while for the same breakdown voltage and temperature  $R_{on}$  is reduced by a factor of ~10 for diamond. [5] This reduction

of on-resistance at elevated temperatures for diamond presents a superior materials characteristics in particular for power electronics. An immediate result emerges for applications at elevated temperatures in the form of reduced or simplified cooling requirements and improved frequency response.

Diamond devices utilizing p-type and n-type layers through boron and phosphorus doping, respectively, typically use electrical contacts based on a Ti/Pt/Au metallurgy. For boron doped diamond a specific contact resistance of  $10^{-4} \Omega \text{ cm}^2$  was reported for a boron doping concentration of  $10^{18} \text{ cm}^{-3}$  and an increase in the boron concentration to  $3 \times 10^{20} \text{ cm}^{-3}$  resulted in a reduced specific contact resistance of  $2 \times 10^{-6} \Omega \text{ cm}^2$ . [6, 7] It was shown that high boron concentrations exceeding  $10^{20} \text{ cm}^{-3}$  can readily be achieved on various crystal orientations. [8, 9, 10, 11, 12] Reliable and practical electrical contacts to p-type diamond can thus be prepared. [13]

Equivalent developments for n-type diamond were challenging because of difficulties in the growth of highly phosphorus doped diamond particularly on (100) oriented surfaces that are preferred for device fabrication. First results for n-type, phosphorus doped, diamond were reported by Koizumi *et al.* where microwave plasma assisted chemical vapor deposition was employed to incorporate phosphorus, from a phosphine source, into a (111) oriented epitaxial layer at a concentration of  $2.5 \times 10^{19} \text{ cm}^{-3}$ . [14] About 8 years later Kato *et al.* reported phosphorus doped, n-type, homoepitaxial diamond on (100) oriented surfaces with a phosphorus doping concentration of  $\sim 2 \times 10^{18} \text{ cm}^{-3}$ . [15] To address the reduced phosphorus incorporation an engineered sample holder was employed to allow increased process gas flow, which resulted in an increased phosphorus incorporation for (111) oriented epitaxial layers up to  $7.4 \times 10^{19} \text{ cm}^{-3}$ . [16] However, heavy phosphorus doping has rarely been reported. In an extensive study where (100) oriented type Ib HPHT diamond substrates with misorientation angles from  $2.1^\circ$  to  $20^\circ$  were used as substrates, a phosphorus incorporation  $> 10^{20} \text{ cm}^{-3}$  was measured for epitaxial layers grown on surfaces with misorientation angles of  $15^\circ$  and  $20^\circ$ . [17] For (111) oriented substrates, Grotjohn *et al.* reported a phosphorus incorporated  $> 10^{20} \text{ cm}^{-3}$  by shifting the microwave plasma enhanced CVD process to a higher deposition pressure of 160 Torr and the deposition temperature to 950-1000°C. [18] With Ti/Pt/Au electrical contacts, a specific contact resistance of  $\sim 4 \Omega \text{ cm}^2$  was presented in the same report. For similar highly phosphorus doped diamond films ([P]  $\sim 10^{20} \text{ cm}^{-3}$ ) an electrical contact was formed through direct surface graphitization of the  $n^+$  layer at 1300 °C in vacuum which established a graphite layer with a thickness of  $\sim 13 \text{ nm}$ . [19] With Ti/Pt/Au contacts in a circular TLM geometry this graphitic layer effected an electrical contact resistance of  $0.9 \Omega \text{ cm}^2$  at 0 V which was reduced to  $\sim 10^{-2} \Omega \text{ cm}^2$  at 3 V. A different approach that addresses the difficulty in obtaining high phosphorus doping concentrations on (100) oriented diamond employed structural modification of the (100) surface through an etching processes to enable growth of (111) crystal facets. This was demonstrated through etching of trenches oriented along [110] directions where the trench-corners presented sites for (111) oriented diamond growth thus

establishing a selective growth process with a phosphorus doping concentration of  $\sim 1 \times 10^{20} \text{ cm}^{-3}$ . Ti based electrical contacts on the regrown surface showed a specific contact resistance of  $\sim 10^{-2} \Omega \text{ cm}^2$ . [20] A variation in this modification of the diamond surface was also achieved through a nickel etching procedure in a hydrogen plasma followed by a nitric acid chemical etch which resulted in inverted pyramid features across the surface. Subsequent microwave plasma CVD growth utilizing tertiarybutyl-phosphine (TBP) resulted in a phosphorus incorporation of  $1\text{-}2 \times 10^{20} \text{ cm}^{-3}$ . [21] This challenge in consistently preparing highly phosphorus doped diamond epitaxial layers and electrical contacts with low electrical contact resistance merits research into approaches that could address present electrical contact limitations.

We present an approach for electrical contacts to n-type, phosphorus doped single-crystal diamond through direct growth of a nanostructured carbon layer with high nitrogen incorporation, that can mitigate reduced phosphorus incorporation in the n-layer and provide one of the lowest specific contact resistances. This contact approach was incorporated in a diamond p-i-n diode used for direct electron emission.

## 2. Experimental

Diamond p-i-n diodes were prepared using 3mm x 3mm x 0.3mm HPHT type IIb plates with (111) surface orientation and a boron concentration of  $\sim 1.2 \times 10^{20} \text{ cm}^{-3}$  indicated by SIMS. These substrates were cleaned by a wet-chemical procedure that commenced with a boil in  $\text{H}_2\text{SO}_4/\text{H}_2\text{O}_2/\text{H}_2\text{O}$ , 3:1:1 at  $220^\circ\text{C}$  for 15 min followed by an HF treatment for 5 min and a final boil in  $\text{NH}_4\text{OH}/\text{H}_2\text{O}_2/\text{H}_2\text{O}$ , 1:1:5 at  $75^\circ\text{C}$  for 15 min. After each step the substrate was rinsed with DI water. The sample was then loaded into a plasma enhanced CVD system based on an ASTeX AX5250 reactor with a custom built, water-cooled sample stage and a base pressure of  $10^{-8}$  Torr achieved through turbo-pumping backed by a dry roots pump. For the intrinsic layer in the p-i-n structure process gas flow was established included 393 sccm of hydrogen, 7 sccm of methane and 0.75 sccm of oxygen. At a deposition pressure of  $\sim 60$  Torr and a microwave power of 1100W a growth temperature of  $750^\circ\text{C}$  -  $850^\circ\text{C}$  was recorded by a dual-wavelength optical pyrometer. The same instrument allowed in-situ observation of the growth process and derivation of the film thickness using interference oscillations. Devices in this study were prepared with an intrinsic diamond layer of  $\sim 5 \mu\text{m}$  thickness. For the phosphorus doped diamond layer the p-i structure was loaded into a similar PECVD system solely used for phosphorus doping. A 200 ppm trimethylphosphine in hydrogen (TMP/ $\text{H}_2$ ) gas mixture was used as the phosphorus source. Prior to phosphorus doped diamond deposition, the surface was exposed for 5 min to a pure hydrogen plasma where a hydrogen flow rate of 400 sccm, a chamber pressure of 65 Torr and a microwave power of 1500 W resulted in a substrate temperature of  $\sim 750^\circ\text{C}$  as measured by a dual-wavelength optical pyrometer. **Adjusting the hydrogen flow rate to 349 sccm and establishing a methane flow rate of 0.25sccm and a 200 ppm TMP in  $\text{H}_2$  flow rate of 50 sccm presented the**

**growth regime for the phosphorus doped diamond layer, which was maintained for 40 min.** This resulted in a film thickness of ~400nm and the p-i-n diode structure that served as a reference for the electrical contact studies. For this contact research an additional layer was grown on the n-layer in a similar PECVD system that is used for nitrogen doped diamond growth. This system employs a rotary vane pump as processing pump and an induction heater utilizing a graphite susceptor. Growth of the contact layer commenced after a 5 min hydrogen plasma cleaning step and utilized a hydrogen flow rate of 400 sccm, a microwave power of 900 W and a chamber pressure of 20 Torr resulting in a temperature of ~ 700°C. The nanostructured carbon contact layer (nanoC) was grown using 5 sccm of hydrogen, 20 sccm of methane, 100 sccm of nitrogen and 10 sccm of argon. With a microwave power of 900 W and a chamber pressure of 20 Torr the substrate temperature was recorded at ~900°C, and the deposition continued for 20 min resulting in a film thickness of ~ 200nm. For electrical contact characterization of the nanoC layer, a film grown with the same processing parameters was prepared on a (100) type IIa CVD diamond substrate using the wet-chemical cleaning procedure as described above.

Devices in this study included circular diodes and pronged-fork geometries. Photo-lithography utilizing an aluminum hard mask was employed for etching the mesa using an O<sub>2</sub>/SF<sub>6</sub> plasma to a depth from 0.5 μm to 3 μm. Electrical contacts were then deposited through e-beam evaporation using Ti/Pt/Au layers with respective thicknesses of 50nm/50nm/150nm, respectively. This processing procedure was compatible with the nanostructured carbon contact layer and its integrity was not adversely affected.

The nano structured carbon film morphology was imaged using an FEI XL30 Environmental Field Emission scanning electron microscope. A secondary electron image was acquired using an accelerating voltage of 15kV and a working distance of 7.6mm.

Raman spectroscopy was performed employing a custom built Raman spectrometer in a 180° geometry. The sample was excited using a 70 mW Ondax® SureLock™ wavelength stabilized diode laser with a wavelength of 633nm. The laser power was controlled using a neutral density filters wheel. The laser was focused onto the sample using a 50X super long working distance plan APO Mitutoyo objective with a numerical aperture of 0.42. The signal was discriminated from the laser excitation using a laser Kaiser® bandpass filter combined with a Semrock RazorEdge® ultrasteep longpass edge filter.

Electrical characterization was performed after a hydrogen passivation of the final device that included exposure of the diamond device die to a pure hydrogen plasma at ~850°C for 5 min. After loading the sample into the electrical characterization chamber, it was evacuated to a base pressure in the mid 10<sup>-9</sup> Torr range. The sample, positioned on a heatable sample stage, was annealed at 600°C for 15 min and after cool-down electrical characterization commenced. Utilizing gold plated probes individual devices were biased up to 20V in forward direction using a Keithley 2400-LV

SourceMeter. An electron collector consisting of a gold plated probe was positioned adjacent to the mesa and a bias varying from 100V to 500V was applied using an SRS PS325 high voltage power supply.

### 3. Results and Discussion

#### 3.1. Diamond p-i-n diodes for electron emission

The observation of direct electron emission from a diamond p-n junction suggested its application as an electron source. [22] Electron sources are widely deployed in space and terrestrial telecommunications through travelling wave-tubes (TWT's) for radar applications, and scientific apparatus like free electron lasers (FEL's), electron microscopes and analytical probing instruments. [23, 24]

Diamond has long been investigated for electron emission applications due to the ability of its surfaces to obtain negative electron affinity characteristics, which shifts the vacuum level below the conduction band minimum (CBM) thus enabling direct release of electrons from the CBM into vacuum. [25, 26, 27] Injecting electrons into the conduction band of a diamond p-i-n diode presents an approach that allows a fraction of the diode current to be emitted into vacuum. The corresponding device, shown schematically in Figure 1, presents a lithographically processed mesa of a layered diamond structure in a p-i-n configuration.

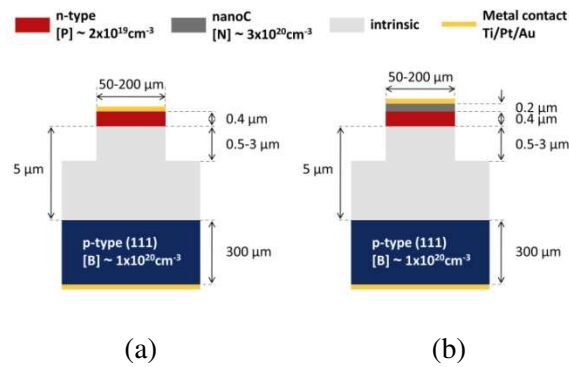


Figure 1. Schematic of a diamond p-i-n diode detailing dimensions and doping concentrations used in this study. The reference structure (a) for the electrical contact research was modified by insertion of a nanostructured carbon (nanoC) layer with high nitrogen incorporation of  $\sim 3 \times 10^{20} \text{cm}^{-3}$  (b).

The diamond p-i-n diode was operated through application of a variable forward bias,  $U_{\text{diode}}$ , across the device. Simultaneously, an electrode was positioned about 100  $\mu\text{m}$  above the diode and biased at  $U_{\text{bias}} = 100\text{V}$  to collect electrons from a single diode. The current,  $I_{\text{diode}}$ , through the diode was varied, and the electron emission current,  $I_{\text{em}}$ , recorded with the bias voltage as a parameter. The corresponding plot shown in Figure 2 (red and black curves) presents data from diodes with 200  $\mu\text{m}$

diameter and a mesa height of 0.5  $\mu\text{m}$  (red curve) and 1  $\mu\text{m}$  (black curve). Under a diode forward bias of  $U_{\text{bias}} = 20\text{V}$ , the diode current was increased up to 400 mA with the electron emission current exceeding 7  $\mu\text{A}$ .

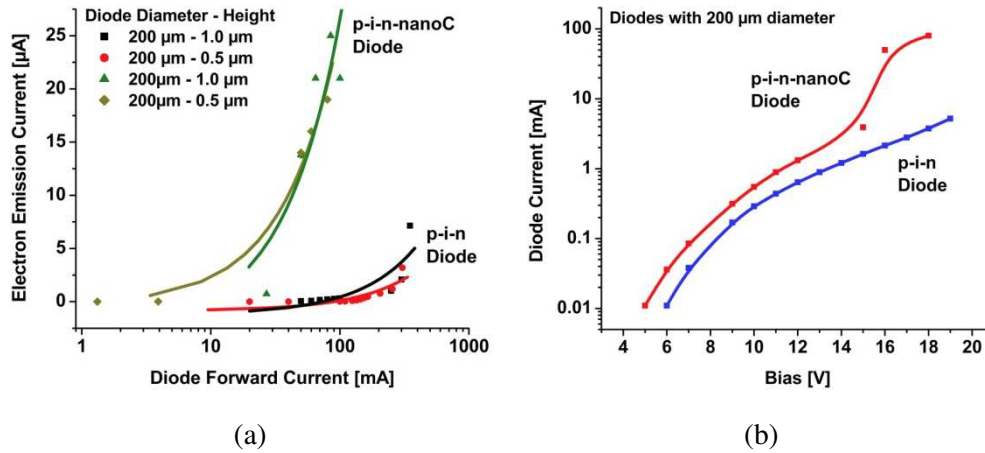


Figure 2. (a) Electron emission from a 200  $\mu\text{m}$  diameter and 0.5 - 1  $\mu\text{m}$  mesa diamond p-i-n diode, biased with  $U_{\text{diode}} = 20\text{V}$ , as a function of diode current (red/black data) and the same characterization for a p-i-n-nanoC diode utilizing a nanostructured carbon (nanoC) contact layer (orange/green data) indicating a significant enhancement in the emission current and a reduced operating voltage of  $U_{\text{diode}} = 16\text{V}$ . (b) Current-voltage characteristics of 200  $\mu\text{m}$  diodes with 1  $\mu\text{m}$  mesa height demonstrating increased current for the nanoC contacted device (red data).

The observed electron emission from the p-i-n structure can partly be related to the generation of excitons which is evidenced by the emission of light from the diode. The recombination of excitons in combination with a transverse-optical (TO) phonon at room temperature effects deep UV emission around 240 nm and broadband emission around 350 nm and 500 nm related to defects and nitrogen states in the intrinsic diamond layer. [28] Excitons in diamond have a radius of 15  $\text{\AA}$  and compared to the nearest-neighbor distance of 1.54  $\text{\AA}$  are considered Mott-Wannier excitons that can freely move in the diamond crystal. With a binding energy of 80 meV these excitons are stable at higher temperatures above 300  $^{\circ}\text{C}$  which is below the operation temperature of the diamond emission diode. The exciton recombination lifetime is typically from micro- to milliseconds, significantly longer than nanoseconds for direct-transition semiconductors. Overall, the observed electron emission current is defined by directly emitted electrons and excitons that diffuse to the NEA surface. [29, 30, 31]

### 3.2. Diamond p-i-n-nanoC diodes for electron emission

In a next step a diamond p-i-n-nanoC diode was prepared by PECVD under the same growth parameters for the epitaxial diamond layers with the same thicknesses and doping concentrations. The same Ti/Pt/Au metallurgy was used and the final structure exposed to a hydrogen plasma.

The first critical observation in the p-i-n-nanoC diode performance was the increased diode current at a reduced forward bias shown in Figure 2 (b) (red data). **A 200  $\mu\text{m}$  diameter diode was biased at 18V in forward direction, and at a diode current of 65 mA an electron emission current of 21  $\mu\text{A}$  was measured.** The corresponding efficiency was calculated to  $2.0 \times 10^{-5} \text{A/W}$ . In a report by Takeuchi *et al.* a diamond p-i-n<sup>+</sup> diode with a phosphorus concentration of  $\sim 10^{20} \text{cm}^{-3}$  was characterized at a forward voltage of 81V establishing a diode current of 5mA and resulting in an emission current of 8.8 $\mu\text{A}$ . [32] Similarly, the efficiency can be calculated as  $2.1 \times 10^{-5} \text{A/W}$ . It should be noted that results from Takeuchi *et al.* targeted a higher emission efficiency for an "inverted" p-i-n<sup>+</sup> diode where a type Ib (111) oriented substrate was used for growth of a heavy phosphorus doped n<sup>+</sup> layer, intrinsic layer, and a top p-type layer with a boron concentration  $< 10^{18} \text{cm}^{-3}$ . The agreement in the comparison of efficiencies for devices prepared with a nanoC and an n<sup>+</sup> layer identifies the importance of the n-type electrical contact for the emission diodes and verifies the viability of the nanoC contact approach.

SIMS characterization of the top section of the p-i-n-nanoC diode indicated a heavy nitrogen doped nanoC layer of  $[\text{N}] > 3 \times 10^{20} \text{cm}^{-3}$  and a moderate phosphorus incorporation of  $\sim 2 \times 10^{19} \text{cm}^{-3}$  for the n-layer as shown in Figure 3 (a). In conjunction with the electrical characterization data of the p-i-n-nanoC and p-i-n<sup>+</sup> diodes, the results further indicate that the highly nitrogen doped nanoC layer can mitigate the high contact resistance due to a reduced doping concentration of the n-layer.

For a quantitative electrical contact analysis an identical nanoC layer was deposited on a type Ila CVD diamond substrate with (100) surface orientation and a pattern for the Transfer Length Method (TLM) was prepared using Ti/Pt/Au metallurgy. The TLM pattern was comprised of rectangular contacts sized  $200 \mu\text{m} \times 300 \mu\text{m}$  that were separated at their longer side by  $d = 10, 20, 30, 50$  and  $100 \mu\text{m}$ . Electrical characterization was performed after the same annealing step used for the p-i-n diodes and in the same UHV characterization system. Figure 3 (b) displays electrical measurements acquired at room temperature (RT) and at  $300^\circ \text{C}$ . Over this temperature range the I/V characteristics were observed to follow a linear dependence with zero crossing. At room temperature Ti/Pt/Au contacts to the nanoC layer were characterized with a specific contact resistance of  $5.5 \times 10^{-3} \Omega \text{cm}^2$ . With an increase in temperature to  $300^\circ \text{C}$  the specific contact resistance decreased to  $4.2 \times 10^{-3} \Omega \text{cm}^2$ . **The measured total resistance,  $R_{\text{total}}$ , can be described in terms of the contact resistance,  $R_C$ , and the sheet resistance,  $R_S$ , by**

$$R_{\text{total}} = 2R_C + \frac{R_S}{W} d \quad (1)$$

with  $W$  the width of the contacts and  $d$  their separation. At room temperature a sheet resistance of  $R_s = 5.7\text{k}\Omega/\square$  was derived and at  $300^\circ\text{C}$  its value decreased to  $R_s = 5\text{k}\Omega/\square$ .

Ohmic contact formation of various metals to nitrogen incorporated nanocrystalline and ultra-nanocrystalline diamond was previously demonstrated with a low contact resistivity of  $200\text{--}380 \times 10^{-3}\ \Omega\ \text{cm}^2$  reported for nickel contacting nitrogen doped nanocrystalline diamond (NCD). [33, 34]

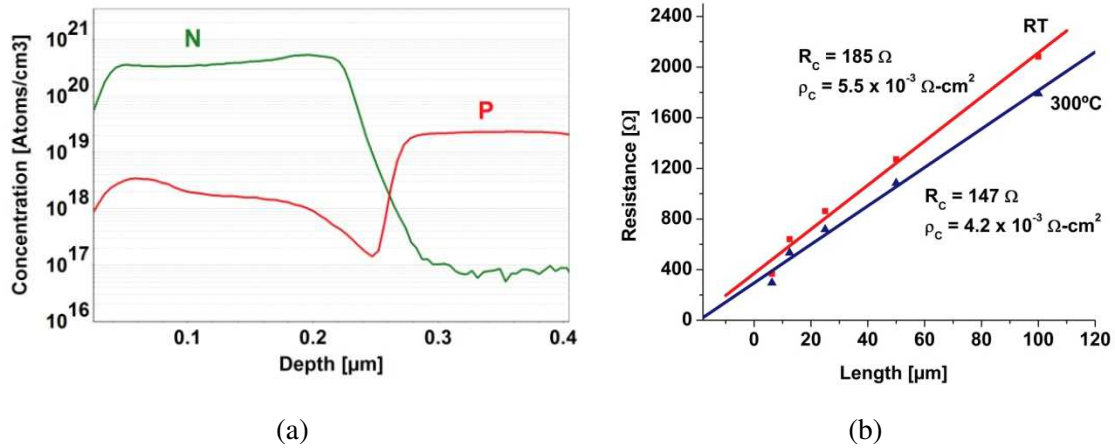


Figure 3. (a) SIMS characterization of the top section of the diamond p-i-n-nanoC diode communicating a high nitrogen incorporation  $>3 \times 10^{20}\ \text{cm}^{-3}$  for the nanoC layer and moderate phosphorus incorporation of  $\sim 2 \times 10^{19}\ \text{cm}^{-3}$  for the n-layer. (b) Electrical characterization in a TLM configuration of a nanostructured carbon layer (nanoC) with high nitrogen incorporation. The low specific contact resistance of  $5.5 \times 10^{-3}\ \Omega\ \text{cm}^2$  at room temperature (RT) is reduced to  $4.2 \times 10^{-3}\ \Omega\ \text{cm}^2$  at  $300^\circ\text{C}$ .

Electrical properties of nanostructured diamond in the form of nanocrystalline (NCD) and ultra-nanocrystalline (UNCD) diamond have been widely discussed in the literature where nitrogen incorporation was typically employed to control electrical conductivity. [35, 36, 37] As nitrogen is preferentially incorporated into the graphitic grain boundaries we suggest a growth regime in a nitrogen rich ambient and under the addition of significant methane flow that was expected to increase the graphitic grain boundary phase in the film and saturate its nitrogen content. [38] Growth of the nanostructured carbon film using the parameters presented in this study resulted in a nitrogen incorporation that maximizes at  $\sim 5 \times 10^{20}\ \text{cm}^{-3}$  which exceeds previously reported results of  $\sim 2 \times 10^{20}\ \text{cm}^{-3}$  for nitrogen incorporated UNCD films. [39, 40] Under the addition of argon a shift in the film morphology to a nanostructured nature was observed and attributed to an increase in the C<sub>2</sub> dimer concentration in the reactant gas phase. [41] Thus, control of the diamond grain size in the film can be achieved through the argon related enhancement of secondary or re-nucleation processes. A scanning electron microscopy image of the same nanostructured carbon (nanoC) film used in this study is depicted in Figure 4. The nanoC film surface exhibits a uniformly structured morphology with

needle-like features with a length limited to  $\sim 500\text{nm}$ . This increased feature size is contrasted by dimensions typically observed in nanocrystalline and ultrananocrystalline diamond films and can be attributed to growth in a nitrogen rich ambient and increased deposition temperatures.

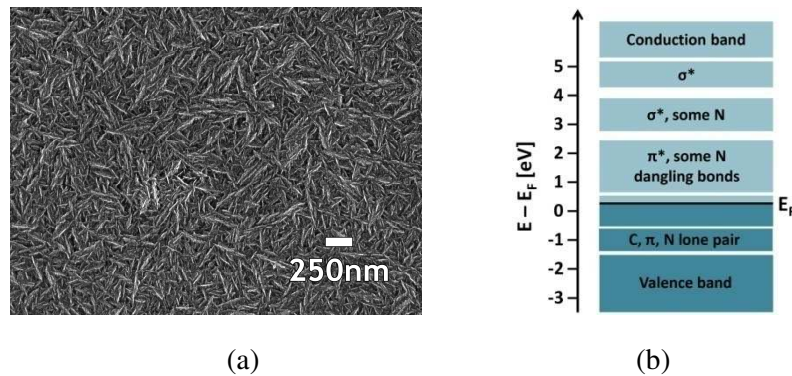


Figure 4. (a) Scanning electron microscopy of a nanostructured carbon (nanoC) film grown on a (111) p-type substrate with deposition conditions of  $\sim 900^\circ\text{C}$  growth temperature, 900 W microwave power, 20 Torr chamber pressure, 5 sccm of hydrogen, 20 sccm of methane, 100 sccm of nitrogen, and 10 sccm of argon. (b) Electronic structure of the grain boundaries with nitrogen incorporation after a simulation by Zapol *et al.* indicating mid-gap states that can advantageously effect electrical contact properties. States below  $E_f - 1.4\text{eV}$  are located in the valence band. [43]

The Raman spectrum of the same nanoC film imaged by scanning electron microscopy in Figure 4(a) is shown in Figure 5. **In diamond a line at  $1333\text{cm}^{-1}$  can be attributed to first order Raman scattering.** With a shift to nanometer sized grains, as observed in nanocrystalline diamond films, a broadening and shift in the diamond line is observed. As the linewidth can be related to the phonon lifetime, its broadening can be attributed to an increase in defects (grain boundaries) and impurities (nitrogen). Disordered graphite effects features at  $1350\text{cm}^{-1}$  and  $1550\text{cm}^{-1}$  which are typically referred to as D and G modes, respectively. [42, 43] A shift of the G-band to higher wavenumbers was related to the nitrogen related variation in the  $\text{sp}^2$ -bonded carbon configuration in the grain boundaries. [44,45] Vibrational modes of trans-polyacetylene (t-PA) can be related to features at  $1140\text{cm}^{-1}$  and  $1480\text{cm}^{-1}$ , corresponding to  $\nu_1$  (C–H in-plane bending) and  $\nu_3$  (C=C stretch) modes, respectively. [46, 47] **These two bands were shown to decrease in intensity with increased nitrogen concentration during growth.** [48]

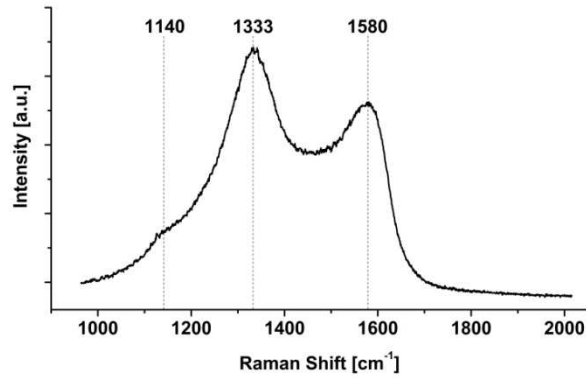


Figure 5. Raman spectrum of the nano structured carbon (nanoC) film (see Figure 4a.) using a laser wavelength of 633nm.

The electronic structure of grain boundaries in UNCD films under nitrogen addition (see Figure 4 (b)) was modeled by Zapol *et al.* in a Tight-binding molecular-dynamics simulation. The results indicated the formation of mid-gap states near and  $\sim 3$  eV above the Fermi level in  $\pi^*$  and  $\sigma^*$  carbon bond configurations, respectively. The states were projected to tail into the conduction band due to distortions in bond geometries. [49] It was further suggested that electrons from carbon dangling bonds, hybridized with nitrogen lone pairs, can transfer to carbon defects near the Fermi level resulting in its upward shift toward the  $\pi^*$  band. With an increase in nitrogen the  $sp^2$  bonded carbon phase is increased resulting in a broadening of the  $\pi$  and  $\pi^*$  states and an increase of their delocalization effects quasimetallic properties. Electronic transport in the grain boundaries can then be described in terms of conduction band conductivity  $\sigma_c$  and hopping conductivity  $\sigma_h$  that requires localized states at the Fermi level. [50, 51] Formation of ohmic contacts is then defined by the mid gap states in the grain boundaries which was demonstrated through etching of the  $sp^2$  carbon phase and deterioration in the ohmic contact behavior. [52]

To establish emission efficiency defining parameters diamond p-i-n-nanoC emission diodes were prepared with varying fork-like geometries as shown in Fig 6. Additionally, the thickness of the nanoC layer was reduced by adjusting the deposition time from 20 min to 15 min, which was expected to reduce the nanoC film thickness from 200 nm to 150 nm. The linear components were fabricated with a trace width  $w$  of 50  $\mu\text{m}$  and 100  $\mu\text{m}$  and with the mesa etched 3  $\mu\text{m}$  into the intrinsic diamond layer. The diamond die, shown in Figure 6 (a), displays individual operating units identified by their light emission. The dimensions of the labeled devices (i), (ii) and (iii), are included in the table.

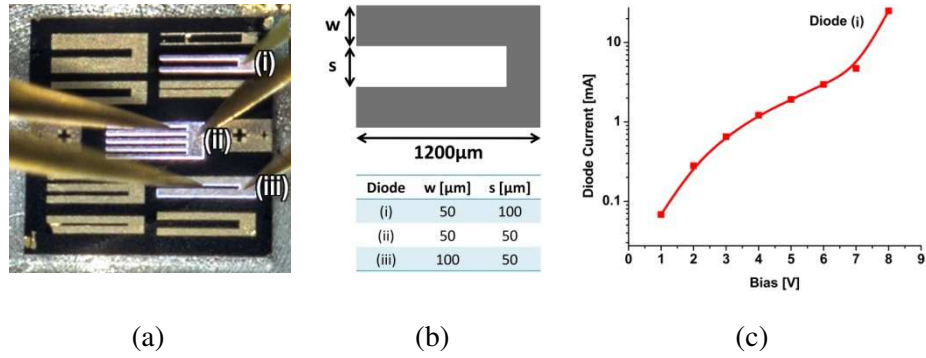


Figure 6. (a) Diamond die (3mm x 3mm) with various p-i-n-nanoC-Ti/Pt/Au emission diodes and their operation indicated by light emission (composite image.) Electrodes on the left side of the image are the electron collector above the diodes. (b) Critical dimensions of three diodes presented in this research with varying trace widths  $w$  of  $50\mu\text{m}$  and  $100\mu\text{m}$ . (c) Current-voltage plot for diode (i); diodes (ii) and (iii) were operated under current compliance.

For the linear structures the same hydrogen passivation and annealing procedures were employed prior to electrical characterization with data plotted in Figure 7. The first critical observation in diode performance is indicated through the significantly reduced operating voltage of 9 V. The I/V plot of diode (i) in Figure 6 (c) indicated a current of 25 mA at a bias of 8V and at a bias of 9 V the diode reached the current compliance level. For device (iii) in Figure 6 (a) a forward current of 200 mA at 9 V bias resulted in an electron emission current of 240  $\mu\text{A}$ . This improvement in electrical diode characteristics, i.e. increased forward current at a reduced bias, is observed for all devices (i), (ii) and (iii) in Figure 6 (a) indicating the high degree of uniformity in the diamond epitaxy and lateral uniformity of the nanoC layer. It furthermore signifies the effects of an optimized nanoC layer, i.e. the electrical contact, where its through-film resistivity reduction can contribute to the increased diode current. With the reduced diode operating voltage of 9V and at a corresponding diode current of 200 mA an emission current of 240  $\mu\text{A}$  corresponds to an efficiency of  $\sim 1.3 \times 10^{-4}$  A/W which is about an order of magnitude higher than emission from the circular device as shown in Figure 7 (a). Furthermore, electron emission measurements of 2-finger and 5-finger devices present superior emission characteristics for the 2-finger device as shown in the blue line in Figure 7 (a). In a next step the 2-finger device was characterized with respect to the finger width ( $w$ ) and the extraction voltage with results plotted in Figure 7 (b).

The current/voltage behavior can generally be described by a power law in the form of  $J \propto V^n$  where an exponent of 1.5 typically indicates space charge limited transport in vacuum, i.e. the Child - Langmuir law. As the extraction voltage is increased from 300 V to 500 V the electron emission current increases with linear dependence as shown in Figure 7 (c). A similar linear emission current behavior was reported by Takeuchi *et al.* for a p-i-n diode operated at a higher diode current of 30 mA. [53] A closer investigation of the electron emission for devices with a trace width,  $w$ , of  $50\mu\text{m}$

and 100  $\mu\text{m}$  indicates an improved emission current for the device with 100  $\mu\text{m}$  wide traces. This observation signifies advantageous effects of emitter geometry and its dimensions for improved efficiencies.

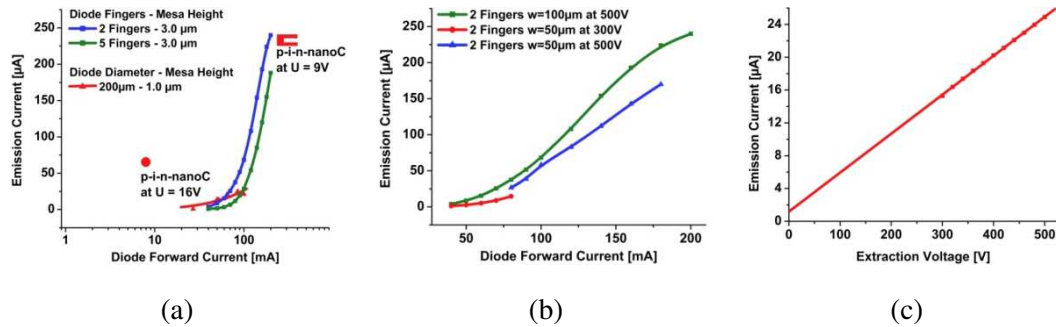


Figure 7. (a) Electron emission current for p-i-n-nanoC diode with circular geometry (red curve) and linear geometry with 2 fingers (blue curve) and 5 fingers (green curve) displaying enhanced electron emission current for 2 finger devices. (b) The electron emission is observed to depend on the trace width  $w$  of the linear emitters where a 100  $\mu\text{m}$  trace width effects an increased emission current. (c) Higher extraction voltages at the collector result in a linear increase in the emission current.

**It should be noted that field emission is not expected to measurably contribute to the total emission current as the applied extraction field is  $<5\text{V}/\mu\text{m}$  and similar nanostructured carbon films required electric fields  $>10\text{V}/\mu\text{m}$  for electron emission. [54] Furthermore, the hydrogen passivation of the final device will effect changes in the nanoC layer through preferential etching of the graphitic carbon phase thus altering its structure that would make it conducive to field emission. Finally, the observation of the emission current's linear dependence on the extraction voltage indicated that typical field emission behavior is not observed in this voltage regime.**

#### 4. A critical overview of electron source efficiencies

The demonstration of practical electron emission sources based on diamond p-i-n diodes warrants an investigation of their competitiveness with currently utilized electron emitter technologies. To establish a measure of efficiency for p-i-n based electron sources we refer to well established devices, x-ray sources, travelling wave tubes (TWT's) and microwave magnetrons, that utilize a cathode (thermionic) and present a comparison in Figure 8.

One of the most basic electron sources can be realized by a tungsten filament. Through direct heating power is dissipated in the wire and an electron current is released through thermionic electron emission. A typical device (HeatWave Labs, Inc., tungsten filament source HWE 5105262) can be characterized by an efficiency of  $\sim 10^{-5}$  A/W, i.e. electron emission current / electrical power

dissipated in the cathode. For a practical apparatus (TOSHIBA Industrial Magnetron 2M164, 1.3 - 1.6 kW, 2.45 GHz) an efficiency for the directly heated thoriated tungsten filament of  $\sim 10^{-2}$  A/W can be derived. Similarly, for typical travelling wavelines to the mm spectrum (Teledyne Microwave Solutions, Continuous Wave TWT MEC 5500E, 400 W, 2 - 6.5 GHz; L3 Electron Devices, Mini-Traveling Wave Tube L6122, 50 W, 30 - 36 GHz) the electron source efficiency is  $\sim 10^{-2}$  A/W. A somewhat lower efficiency was derived for an industrial x-ray source (Varex Imaging Corporation, Industrial X-Ray Tube OEG-83J) utilizing a toroidal, tungsten based electron source with an efficiency of  $\sim 10^{-3}$  A/W. It should be noted that for devices where the anode current  $I_a$  was specified we assumed  $I_a = (1 - \alpha) I_c$ , with  $I_c$  the emission current from the cathode and  $\alpha$  typically in the range 0.65 - 0.75. [55] Takeuchi *et al.* demonstrated a high voltage vacuum switch utilizing a p-i-n diode with an intrinsic diamond layer thickness of 40  $\mu\text{m}$ , a 350  $\mu\text{m}$  thick p-layer with a boron doping concentration of  $3 \times 10^{17} \text{ cm}^{-3}$  and a 200 nm thick n-layer with a phosphorus doping concentration of  $1 \times 10^{20} \text{ cm}^{-3}$ . Under a forward bias of 25 V a diode current of 35mA was established and an emission current of 0.91 mA presented an efficiency of  $1 \times 10^{-3}$  A/W. [56]

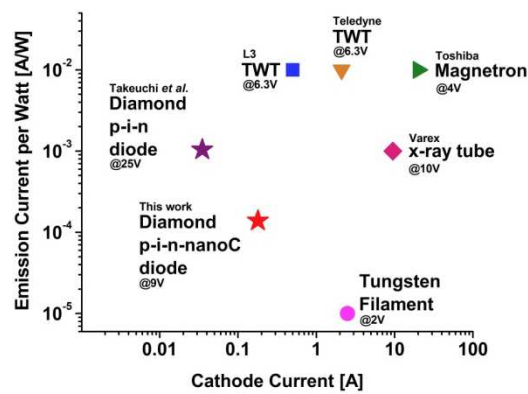


Figure 8. Comparison of various electron sources utilized in practical devices detailed in the text. The cathode current in the plot presents the current operating the diamond diode and the thermionic electron source through direct/indirect heating. The operating voltage of the cathode is represented in the horizontal axis.

## 5. Conclusions

We have demonstrated a contact approach to phosphorus doped, n-type diamond, by direct growth of a high nitrogen incorporated nanostructured carbon (nanoC) layer. With a maximum nitrogen concentration of  $\sim 5 \times 10^{20} \text{ cm}^{-3}$  this nanoC layer can mitigate reduced phosphorus incorporation of the n-layer and using Ti/Pt/Au contact metallurgy provide a low specific contact resistance of  $5.5 \times 10^{-3} \Omega \text{ cm}^2$  at room temperature. This low value was in part attributed to the electronic structure in the nanoC

grain boundaries that can effect quasimetallic materials characteristics. Application of this nanoC contact approach in a diamond p-i-n-nanoC diode for electron emission demonstrated its viability for devices exceeding conventional approaches presented for p-i-n<sup>+</sup> diode with a phosphorus concentration of  $\sim 10^{20}\text{cm}^{-3}$ .

We acknowledge the use of facilities within the Eyring Materials Center at Arizona State University supported in part by NNCI-ECCS-1542160.

This research was support by the Office of Naval Research under grant #N00014-17-1-3002, and the National Science Foundation under grant #IIP - 1747133

#### References:

- [1] Diamond as an electronic material, Chris J.H. Wort, Richard S. Balmer, *Materials Today*, Volume 11, Issues 1–2, 2008, Pages 22-28.
- [2] *Fundamentals of Power Semiconductor Devices*, B. Jayant Baliga, Springer Science & Business Media, 2010, ISBN 0387473149.
- [3] Lower limits to metal-semiconductor contact resistance: Theoretical models and experimental data, Baraskar, Ashish, A. C. Gossard, and Mark JW Rodwell, *Journal of Applied Physics* 114, no. 15 (2013): 154516.
- [4] H. Kang and F. Udreă, "True Material Limit of Power Devices—Applied to 2-D Superjunction MOSFET," in *IEEE Transactions on Electron Devices*, vol. 65, no. 4, pp. 1432-1439, April 2018. doi: 10.1109/TED.2018.2808181
- [5] **High temperature application of diamond power device, Umezawa, Hitoshi, Masanori Nagase, Yukako Kato, and Shin-ichi Shikata, *Diamond and related materials* 24 (2012): 201-205.**
- [6] Investigation of specific contact resistance of ohmic contacts to B-doped homoepitaxial diamond using transmission line model, Chen, Y. G., M. Ogura, S. Yamasaki, and H. Okushi, *Diamond and related materials* 13, no. 11-12 (2004): 2121-2124.
- [7] Electrical and mechanical characterisation of Si/Al ohmic contacts on diamond, Civrac, G., Sabeur Msolli, Joël Alexis, Olivier Dalverny, and Henri Schneider, *Electronics letters* 46, no. 11 (2010): 791-793.
- [8] Properties of boron-doped epitaxial diamond films, Fujimori, Naoji, Hideaki Nakahata, and Takahiro Imai, *Japanese Journal of Applied Physics* 29, no. 5R (1990): 824.
- [9] Characterization of boron-doped diamond epitaxial films, Shiomi, Hiromu, Yoshiki Nishibayashi, and Naoji Fujimori, *Japanese journal of applied physics* 30, no. 7R (1991): 1363.

- [10] Properties of boron-doped epitaxial diamond layers grown on (110) oriented single crystal substrates, Mortet, Vincent, Julien Pernot, François Jomard, Ali Soltani, Zdenek Remes, Julien Barjon, J. D'Haen, and Ken Haenen, *Diamond and Related Materials* 53 (2015): 29-34.
- [11] The effect of substrate temperature and growth rate on the doping efficiency of single crystal boron doped diamond, Demlow, Shannon Nicley, Robert Rechenberg, and Timothy Grotjohn, *Diamond and related materials* 49 (2014): 19-24.
- [12] Raman characterization of boron-doped {111} homoepitaxial diamond layers, Mermoux, Michel, F. Jomard, C. Tavares, Franck Omnès, and Etienne Bustarret, *Diamond and related materials* 15, no. 4-8 (2006): 572-576.
- [13] Ohmic contacts on p-type homoepitaxial diamond and their thermal stability, Yigang Chen, Masahiko Ogura, Satoshi Yamasaki and Hideyo Okushi, *Semicond. Sci. Technol.* 20 (2005) 860–863
- [14] Growth and characterization of phosphorous doped {111} homoepitaxial diamond thin films, Koizumi, S., M. Kamo, Y. Sato, H. Ozaki, and T. Inuzuka, *Applied physics letters* 71, no. 8 (1997): 1065-1067.
- [15] n-type doping of (001)-oriented single-crystalline diamond by phosphorus, Kato Hiromitsu, Satoshi Yamasaki, and Hideyo Okushi, *Applied Physics Letters* 86, no. 22 (2005): 222111.
- [16] Large improvement of phosphorus incorporation efficiency in n-type chemical vapor deposition of diamond, Ryota Ohtani, Takashi Yamamoto, Stoffel D. Janssens, Satoshi Yamasaki, and Satoshi Koizumi, *Applied Physics Letters* 2014 105:23
- [17] Desorption time of phosphorus during MPCVD growth of n-type (001) diamond, Kawashima, Hiroyuki, Hiromitsu Kato, Masahiko Ogura, Daisuke Takeuchi, Toshiharu Makino, and Satoshi Yamasaki, *Diamond and Related Materials* 64 (2016): 208-212.
- [18] Heavy phosphorus doping by epitaxial growth on the (111) diamond surface, Grotjohn, T. A., D. T. Tran, M. K. Yaran, S. N. Demlow, and T. Schuelke, *Diamond and Related Materials* 44 (2014): 129-133.
- [19] Reduction of n-type diamond contact resistance by graphite electrode, Matsumoto, Tsubasa, Hiromitsu Kato, Norio Tokuda, Toshiharu Makino, Masahiko Ogura, Daisuke Takeuchi, Hideyo Okushi, and Satoshi Yamasaki, *physica status solidi (RRL)–Rapid Research Letters* 8, no. 2 (2014): 137-140.
- [20] Selective Growth of Buried n+ Diamond on (001) Phosphorus-Doped n-Type Diamond Film, Hiromitsu Kato, Toshiharu Makino, Masahiko Ogura, Norio Tokuda, Hideyo Okushi, and Satoshi Yamasaki, *Applied Physics Express* 2 (2009) 055502

- [21] New Process for Electrical Contacts on (100) N-type Diamond, Nephi Temahuki, Remi Gillet, Vincent Sallet, Francois Jomard, Ekaterina Chikoidze, Yves Dumont, Marie-Amandine Pinault-Thaury, and Julien Barjon, *Phys. Status Solidi A* 2017, 214, 1700466
- [22] Kono, Shozo, and Satoshi Koizumi. "Images and energy distributions of electrons emitted from a diamond pn-junction diode." *e-Journal of Surface Science and Nanotechnology* 7 (2009): 660-66
- [23] J. H. Booske et al., "Vacuum Electronic High Power Terahertz Sources," in *IEEE Transactions on Terahertz Science and Technology*, vol. 1, no. 1, pp. 54-75, Sept. 2011.
- [24] D. K. Abe, D. R. Whaley, J. Feng, J. Jelonnek and L. Kumar, "Guest Editorial Special Issue on Vacuum Electronics," in *IEEE Transactions on Electron Devices*, vol. 65, no. 6, pp. 2058-2060, June 2018.
- [25] Negative-electron-affinity effects on the diamond (100) surface, J. van der Weide, Z. Zhang, P. K. Baumann, M. G. Wensell, J. Bernholc, and R. J. Nemanich, *Phys. Rev. B* 50, 5803–5806 (1994)
- [26] Angle-resolved photoemission of diamond (111) and (100) surfaces; negative electron affinity and band structure measurements, J. van der Weide and R. J. Nemanich, *J. Vac. Sci. Technol. B* 12, 2475 (1994)
- [27] Quantum photoyield of diamond(111)—A stable negative-affinity emitter, F. J. Himpsel, J. A. Knapp, J. A. VanVechten, and D. E. Eastman, *Phys. Rev. B* 20, 624–627 (1979)
- [28] Electrical and light-emitting properties of homoepitaxial diamond p–i–n junction, Makino, Toshiharu, Norio Tokuda, Hiromitsu Kato, Shokichi Kanno, Satoshi Yamasaki, and Hideyo Okushi, *physica status solidi (a)* 205, no. 9 (2008): 2200-2206.
- [29] Photoelectron emission from diamond, Takeuchi, D., C. E. Nebel, and S. Yamasaki, *physica status solidi (a)* 203, no. 12 (2006): 3100-3106.
- [30] Photoelectron emission properties of hydrogen terminated intrinsic diamond, Takeuchi, D., C. E. Nebel, and S. Yamasaki, *J. Appl. Phys.* 99, (2006): 086102.
- [31] Photoelectric emission from negative-electron-affinity diamond (111) surfaces: Exciton breakup versus conduction-band emission, Bandis, C., and B. B. Pate, *Physical Review B* 52, no. 16 (1995): 12056.
- [32] Electron Emission from a Diamond (111) p–i–n+ Junction Diode with Negative Electron Affinity during Room Temperature Operation, Takeuchi, Daisuke, Toshiharu Makino, Hiromitsu Kato, Masahiko Ogura, Norio Tokuda, Kazuhiro Oyama, Tsubasa Matsumoto, Izumi Hirabayashi, Hideyo Okushi, and Satoshi Yamasaki, *Applied physics express* 3, no. 4 (2010): 041301.
- [33] Electrical contacts to nanocrystalline diamond films studied at high temperatures, Shimoda, Naotaka, Yoshimine Kato, and Kungen Teii, *Journal of Applied Physics* 120, no. 23 (2016): 235706.

- [34] Electrical contacts to ultrananocrystalline diamond, Gerbi, J. E., O. Auciello, J. Birrell, D. M. Gruen, B. W. Alphenaar, and J. A. Carlisle, *Applied physics letters* 83, no. 10 (2003): 2001-2003.
- [35] Structural and electrical properties of nanocrystalline diamond (NCD) heavily doped by nitrogen, Liu, Y. K., P. L. Tso, D. Pradhan, I. N. Lin, M. Clark, and Y. Tzeng, *Diamond and related materials* 14, no. 11-12 (2005): 2059-2063.
- [36] The structure and electrochemical behavior of nitrogen-containing nanocrystalline diamond films deposited from CH<sub>4</sub>/N<sub>2</sub>/Ar mixtures, Chen, Qingyun, Dieter M. Gruen, Alan R. Krauss, Timothy D. Corrigan, Malgorzata Witek, and Greg M. Swain, *Journal of The Electrochemical Society* 148, no. 1 (2001): E44-E51.
- [37] n-Type conductivity in ultrananocrystalline diamond films, Williams, Oliver A., Stephane Curat, Jennifer E. Gerbi, Dieter M. Gruen, and Richard B. Jackman, *Applied Physics Letters* 85, no. 10 (2004): 1680-1682.
- [38] Bonding structure in nitrogen doped ultrananocrystalline diamond, Birrell, James, J. E. Gerbi, O. Auciello, J. M. Gibson, D. M. Gruen, and J. A. Carlisle, *Journal of Applied Physics* 93, no. 9 (2003): 5606-5612.
- [39] Synthesis and characterization of highly-conducting nitrogen-doped ultrananocrystalline diamond films, Bhattacharyya, S., O. Auciello, J. Birrell, J. A. Carlisle, L. A. Curtiss, A. N. Goyette, D. M. Gruen et al., *Applied Physics Letters* 79, no. 10 (2001): 1441-1443.
- [40] Diamond nanowires and the insulator-metal transition in ultrananocrystalline diamond films, Arenal, R., P. Bruno, D. J. Miller, M. Bleuel, J. Lal, and D. M. Gruen, *Physical Review B* 75, no. 19 (2007): 195431.
- [41] Control of diamond film microstructure by Ar additions to CH<sub>4</sub>/H<sub>2</sub> microwave plasmas, Zhou, D., D. M. Gruen, L. C. Qin, T. G. McCauley, and A. R. Krauss, *Journal of Applied Physics* 84, no. 4 (1998): 1981-1989.
- [42] Raman spectrum of graphite, F. Tuinstra, J.L. Koenig, *J. Chem. Phys.* 53 (1970) 1126.
- [43] Origin of the 1150cm<sup>-1</sup> Raman mode in nanocrystalline diamond, Ferrari, A. C., and J. Robertson, A.C. Ferrari, J. Robertson, *Phys. Rev. B* 63 (2001) 121405.
- [44] Bulk and surface-enhanced Raman spectroscopy of nitrogen-doped ultrananocrystalline diamond films, I.I. Vlasov, V.G. Ralchenko, E. Goovaerts, A.V. Saveliev, M.V. Kanzyuba, *Phys. Status Solidi A* 203 (12) (2006) 3028–3035.
- [45] Bonding structure in nitrogen doped ultrananocrystalline diamond, J. Birrell, J.E. Gerbi, O. Auciello, J.M. Gibson, D.M. Gruen, J.A. Carlisle, , *J.Appl. Phys.* 93 (2003) 5606.
- [46] Polyacetylene in diamond films evidenced by surface enhanced Raman scattering, T. Lopez-Rios, E. Sandre', S. Leclerq, and E. Sauvain, *Phys. Rev. Lett.* 76, 4935 (1996).

[47] The mystery of the 1140cm<sup>-1</sup> Raman line in nanocrystalline diamond films, H. Kuzmany, R. Pfeiffer, N. Salk, and B. Gunther, *Carbon* 42, 911 (2004).

**[48] Vibrational properties of nitrogen-doped ultrananocrystalline diamond films grown by microwave plasma CVD, Vlasov, I. I., E. Goovaerts, V. G. Ralchenko, V. I. Konov, A. V. Khomich, and M. V. Kanzyuba, *Diamond and Related Materials* 16, no. 12 (2007): 2074-2077.**

[49] Tight-binding molecular-dynamics simulation of impurities in ultrananocrystalline diamond grain boundaries, Zapol, Peter, Michael Sternberg, Larry A. Curtiss, Thomas Frauenheim, and Dieter M. Gruen, *Physical Review B* 65, no. 4 (2001): 045403.

[50] Effect of nitrogen on the electronic properties of ultrananocrystalline diamond thin films grown on quartz and diamond substrates, Achatz, P., Oliver Aneurin Williams, P. Bruno, D. M. Gruen, J. A. Garrido, and M. Stutzmann, *Physical Review B* 74, no. 15 (2006): 155429.

[51] Mechanism of high n-type conduction in nitrogen-doped nanocrystalline diamond, Bhattacharyya, Somnath, *Physical Review B* 70, no. 12 (2004): 125412.

[52] Electrical contacts to nitrogen incorporated nanocrystalline diamond films, Jeedigunta, Sathyaharish, Priscila Spagnol, John Bumgarner, and Ashok Kumar, *Diamond and Related Materials* 17, no. 12 (2008): 2037-2040.

[53] High-voltage vacuum switch with a diamond p-i-n diode using negative electron affinity, Takeuchi, Daisuke, Toshiharu Makino, Hiromitsu Kato, Masahiko Ogura, Hideyo Okushi, Hiromichi Ohashi, and Satoshi Yamasaki, *Japanese Journal of Applied Physics* 51, no. 9R (2012): 090113.

**[54] Substrate temperature effects on the electron field emission properties of nitrogen doped ultra-nanocrystalline diamond, Chen, Y. C., N. H. Tai, and I. N. Lin, *Diamond and Related Materials* 17, no. 4-5 (2008): 457-461.**

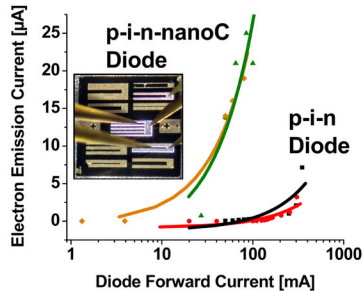
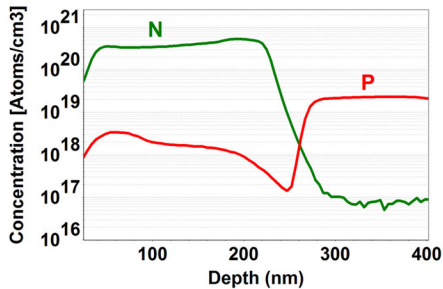
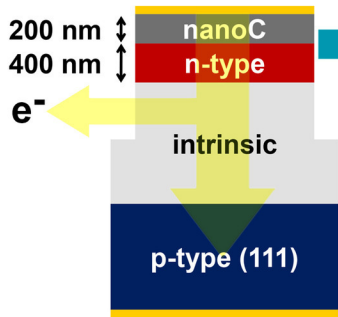
[55] Microwave and RF vacuum electronic power sources, Richard G Carter, Cambridge University Press, 2018.

[56] 4 A/cm<sup>2</sup>, 7kV normally-off diamond-emitter vacuum switch, Takeuchi, D., H. Kawashima, D. Kuwabara, T. Makino, H. Kato, M. Ogura, H. Ohashi, H. Okushi, S. Yamasaki, and S. Koizumi, *2015 IEEE 27th International Symposium on Power Semiconductor Devices & IC's (ISPSD)*, pp. 197-200. IEEE, 2015.

# Diamond p-i-n-nanoC Diode

# SIMS

# Electron Emission



Electrical contact resistivity  
 $\rho_c \sim 5.5 \times 10^{-3} \Omega \text{ cm}^2$